Photoelectron spin polarization in the $Bi_2Te_3(0001)$ topological insulator: Initial- and final-state effects in the photoemission process

Christoph Seibel,[1] Jürgen Braun,[2] Henriette Maaß,[1] Hendrik Bentmann,[1,*] Jan Minár,[2,3] Tatyana V. Kuznetsova,[4,5] Konstantin A. Kokh,[6,7,8] Oleg E. Tereshchenko,[6,7,9] Taichi Okuda,[10] Hubert Ebert,[2] and Friedrich Reinert[1]

[1]*Experimentelle Physik VII and Röntgen Research Center for Complex Materials (RCCM), Universität Würzburg, Am Hubland, D-97074 Würzburg, Germany*

[2]*Department Chemie, Physikalische Chemie, Universität München, Butenandtstrasse 5-13, D-81377 München, Germany*

[3]*New Technologies-Research Center, University of West Bohemia, Univerzitni 8, 306 14 Pilsen, Czech Republic*

[4]*M. N. Miheev Institute of Metal Physics UB RAS, 620990, S. Kovalevskaya Street 18, Ekaterinburg, Russia*

[5]*Ural Federal University, 620002, Mira Street 19, Ekaterinburg, Russia*

[6]*Saint Petersburg State University, 198504, Saint Petersburg, Russia*

[7]*Novosibirsk State University, 636090, Novosibirsk, Russia*

[8]*V.S. Sobolev Institute of Geology and Mineralogy, SB RAS, 630090, Novosibirsk, Russia*

[9]*Institute of Semiconductor Physics, 636090 Novosibirsk, Russia*

[10]*Hiroshima Synchrotron Radiation Center, Hiroshima University, Kagamiyama 2-313, Higashi-Hiroshima 739-0046, Japan*

(Received 2 February 2016; revised manuscript received 8 May 2016; published 27 June 2016)

The photoelectron spin polarization in angle-resolved photoemission from the topological surface state in $Bi_2Te_3(0001)$ has been investigated in a combined experimental and theoretical study. Our measurements show significant photon-energy-dependent deviations in the three-dimensional spin polarization of the photoelectron when compared to the expected intrinsic spin polarization of the surface state. The experimental observations are in line with relativistic one-step photoemission calculations. Our theoretical analysis confirms that spin-orbit coupling in the initial-state wave functions in combination with the dipole selection rules strongly influences the photoelectron spin polarization. Furthermore, spin-dependent final-state effects are found to influence the spin polarization significantly. A quantitative access to the three-dimensional spin-polarization vector in topological insulators is thus challenged by a complex interplay of initial- and final-state effects in the photoemission process.

DOI: 10.1103/PhysRevB.93.245150

I. INTRODUCTION

Topological insulators are currently attracting broad interest in condensed matter physics and are considered for future applications in spintronics and quantum computation [1–4]. The bulk band structure of these materials is characterized by a nontrivial topology that implies the existence of spin-polarized surface states spanning the bulk band gap. The band dispersion of these surface states can be determined experimentally by use of angle-resolved photoelectron spectroscopy (ARPES). This experimental technique therefore constitutes a valuable method for the investigation of topological insulators [5,6]. Furthermore, the detection of the photoelectron spin in a spin-resolved ARPES measurement allows one to address the momentum-dependent spin polarization of topological surface states [7–16]. This is highly desirable, as the locking of spin and momentum represents one of the key features in the surface electronic structure of topological insulators. A different spectroscopic access to the intrinsic spin polarization has also been explored based on the use of circularly polarized light for photoelectron excitation [14,17,18]. However, the resulting dichroic signal turned out to be strongly influenced by the final state in the photoemission process. It thus stands in no immediate relation to the spin polarization of the surface state [19–21]. On the other hand, recent spin-resolved ARPES studies of the topological insulator Bi_2Se_3 also revealed pronounced dependences of the photoelectron spin polarization on energy and polarization of the exciting light [22–26]. This implies considerable influences of the photoemission process on the photoelectron spin in these materials [27].

In general, spin-orbit coupling is known to give rise to spin-polarized photoelectrons from atoms and nonmagnetic solids for excitation with circularly polarized light [28–30], but also for linear polarization if photoelectrons are detected under well-defined angles [31–34]. The latter case can, for example, result from phase shifts in the photoelectron final state, where interference between partial waves of different orbital angular momentum takes place [35], or from spin-dependent photoelectron scattering at the surface [36]. However, spin-polarized photoelectrons from spin-degenerate electronic states can also arise purely due to spin-orbit coupling in the initial state in combination with the finite probing depth of the photoemission experiment [37,38]. In the case of topological surface states, or similarly also for conventional surface states with Rashba-type spin splitting [8], the initial-state wave function is spin polarized. Nevertheless, in the presence of strong spin-orbit interaction, a key ingredient for the formation of topological insulators, considerable mixing between spin-up and spin-down states occurs [39–42], yielding wave functions of the form $\psi = a\phi_\uparrow(\mathbf{r})|\uparrow\rangle + b\phi_\downarrow(\mathbf{r})|\downarrow\rangle$. Hence, differences in the photoemission cross sections of $\phi_\uparrow$ and $\phi_\downarrow$ depending on photon energy and polarization can affect the degree of photoelectron spin polarization [25–27,43,44]. Furthermore, the coherent excitation of spin-up and spin-down electrons may also modify the orientation of the photoelectron spin with respect to the spin-orientation of the initial state [26,39], given

*Corresponding author: hendrik.bentmann@physik.uni-wuerzburg.de

by the expectation value of the spin operator for the initial state.

In this work we investigate the relevance of initial- and final-state effects in the photoemission process for the photoelectron spin polarization in the topological insulator Bi_2Te_3. To this end we compare spin-resolved ARPES measurements of the three-dimensional spin-polarization vector of the topological surface state (TSS) to the results of relativistic one-step photoemission calculations, taking into account transition matrix elements and multiple scattering. The experimental and theoretical results consistently indicate significant photon-energy-dependent modifications of the photoelectron spin-polarization as compared to the expected spin-polarization of the initial state. While we find that spin-orbit coupling in the initial-state wave functions plays an important role for these modifications our analysis also reveals that spin-dependent effects in the final state considerably influence the photoelectron spin polarization.

II. METHODOLOGY

A. Experiment

The experiments were performed at the efficient spin resolved spectroscopy observation end station (ESPRESSO) at the Hiroshima synchrotron radiation center (HiSOR BL-9B) [45]. The Bi_2Te_3 single crystal, grown by a modified vertical Bridgman method [46], was cleaved along the (0001) direction under ultrahigh vacuum (UHV) conditions at room temperature. It was subsequently cooled down to the measurement temperature of $T \approx 40$–70 K. A Scienta R4000 hemispherical photoelectron spectrometer was utilized at pressures below 4×10^{-10} mbar during the measurements. The spin detector is based on very low energy electron diffraction (VLEED) and projects the photoelectron spin to the variable axis of magnetization $\mathbf{M}$ of the target surface [45,47]. The spin-resolved photoemission intensities $I_{\uparrow\downarrow}(E,k)$ are obtained from the scattering asymmetry $A(E,k) = \frac{I_{+\mathrm{M}} - I_{-\mathrm{M}}}{I_{+\mathrm{M}} + I_{-\mathrm{M}}} = \frac{I_{+\mathrm{M}} - I_{-\mathrm{M}}}{I_{\mathrm{total}}}$ via

$$I_{\uparrow\downarrow}(E,k) = [1 \pm P(E,k)]\frac{I_{\mathrm{total}}(E,k)}{2}, \tag{1}$$

where the photoelectron spin polarization $P(E,k)$ along a given direction in space is given by

$$P(E,k) = \frac{1}{S}A(E,k). \tag{2}$$

The Sherman function of the detector was $S = 0.3$. The high symmetry directions as well as the directions of measurements where identified by determination of the electronic band structure and the Fermi surface. The measurements were performed using p-polarized light.

B. Theoretical and computational background

We start with Pendry's formula for the photocurrent which defines the one-step model of PES [48]:

$$I^{\mathrm{PES}} = -\frac{1}{\pi}\Im\ \langle \epsilon_f, \mathbf{k}_\parallel | G_2^+ \Delta G_1^+ \Delta^\dagger G_2^- | \epsilon_f, \mathbf{k}_\parallel \rangle\ . \tag{3}$$

The expression can be derived from Fermi's golden rule for the transition probability per unit time [49]. Consequently, I^{PES} denotes the elastic part of the photocurrent. Vertex renormalizations are neglected. This excludes inelastic energy losses and corresponding quantum-mechanical interference terms [48–50]. Furthermore, the interaction of the outgoing photoelectron with the rest system is not taken into account. This "sudden approximation" is expected to be justified for not too small photon energies.

We consider an energy-, angle-, and spin-resolved photoemission experiment. The state of the photoelectron at the detector is written as $|\epsilon_f, \mathbf{k}_\parallel\rangle$, where $\mathbf{k}_\parallel$ is the component of the wave vector parallel to the surface, and ϵ_f is the kinetic energy of the photoelectron. The spin state of the photoelectron is implicitly included in $|\epsilon_f, \mathbf{k}_\parallel\rangle$ which is understood as a four-component Dirac spinor. The advanced Green function G_2^- in Eq. (3) characterizes the scattering properties of the material at the final-state energy $E_2 \equiv \epsilon_f$. Via $|\Psi_f\rangle = G_2^-|\epsilon_f, \mathbf{k}_\parallel\rangle$ all multiple-scattering corrections are formally included. The operator Δ mediates the coupling to the electromagnetic field.

For an appropriate description of the photoemission process, we must ensure the correct asymptotic behavior of $\Psi_f(\mathbf{r})$ beyond the crystal surface, i.e., a single outgoing plane wave characterized by ϵ_f and $\mathbf{k}_\parallel$. Furthermore, the damping of the final state due to the imaginary part of the inner potential $iV_{0\mathrm{i}}(E_2)$ must be taken into account. We thus construct the final state within spin-polarized low-energy electron diffraction (SPLEED) theory considering a single plane wave $|\epsilon_f, \mathbf{k}_\parallel\rangle$ advancing onto the crystal surface. Using standard LEED techniques [51], generalized for the relativistic case [52,53], we first obtain the SPLEED state $U\Psi_f(\mathbf{r})$. The final state is then given as the time-reversed SPLEED state ($U = -i\sigma_y K$ is the relativistic time inversion). Many-body effects are included phenomenologically in the SPLEED calculation by using a parametrized, weakly energy-dependent and complex inner potential $V_0(E_2) = V_{0\mathrm{r}}(E_2) + iV_{0\mathrm{i}}(E_2)$ as usual [51]. This generalized inner potential takes into account inelastic corrections to the elastic photocurrent [49] as well as the actual (real) inner potential, which serves as a reference energy inside the solid with respect to the vacuum level [54]. Due to the finite imaginary part $iV_{0\mathrm{i}}(E_2)$, the flux of elastically scattered electrons is permanently reduced, and thus the amplitude of the high-energy wave field $\Psi_f(\mathbf{r})$ can be neglected beyond a finite distance from the surface. This way the one-step description of the photoemission process includes all matrix-element effects, all multiple scattering effects in the initial and final states, and the effect of the photon momentum vector.

To disentangle explicitly matrix-element effects from surface and final-state effects, we introduce the spectral function representation of Pendry's formula, which allows for an explicit illustration of final-state effects [20]. The spectral function representation can be written as

$$-\frac{1}{\pi}\Im G_1^+ = \sum_i B_{ii}|\Psi_i\rangle\langle\Psi_i|, \tag{4}$$

where the Green's function for the photohole is given as a sum (integral over k_z for all bands) of spectral functions B_{ii} over initial states. The ARPES intensity can now be expressed formally as

$$I(\epsilon_f, \mathbf{k}_\parallel) = \sum_i B_{ii}|\langle\Psi_f|\Delta|\Psi_i\rangle|^2. \tag{5}$$

The initial and final states can be written in spherical harmonic representation according to [48,55]

$$\Psi_i = \sum_{\kappa\mu} A_{1\kappa\mu} R_\kappa(k_i r)\chi_{\kappa\mu}(\theta,\phi),$$
$$\Psi_f = \sum_{\kappa'\mu'} A_{2\kappa'\mu'} R_{\kappa'}(k_f r)\chi_{\kappa'\mu'}(\theta,\phi). \quad (6)$$

Here the complex expansion coefficients

$$A_{1\kappa\mu} = |A_{1\kappa\mu}|e^{i\delta_{\kappa\mu}} \quad \text{and}$$
$$A_{2\kappa'\mu'} = |A_{2\kappa'\mu'}|e^{i\delta_{\kappa'\mu'}} \quad (7)$$

contain the corresponding relative phases $\delta_{\kappa\mu}$ and $\delta_{\kappa'\mu'}$ of the relativistic partial waves $\kappa\mu$ and $\kappa'\mu'$, where $\kappa\mu$ are the relativistic quantum numbers and $\chi_{\kappa\mu}$ denotes a relativistic spin-angular function [52].

If we fix for a moment the initial-state coefficients to $A_{1\kappa\mu} = 1$ in order to study the final-state effects only [20], we get for the intensity signal

$$I^{\mathrm{PES}} \approx \mathrm{Im} \sum_{\kappa\mu\kappa'\mu'\kappa''\mu''} M_{\kappa,\kappa'} M^*_{\kappa',\kappa''} D_{\kappa\mu\kappa'\mu'} D^*_{\kappa'\mu'\kappa''\mu''}$$
$$\times |A_{2\kappa\mu}||A_{2\kappa''\mu''}|e^{i(\delta_{2\kappa\mu}-\delta_{2\kappa''\mu''})}, \quad (8)$$

where the relativistic angular matrix elements $D_{\kappa\mu\kappa'\mu'}$ take care of the dipole selection rules. $M_{\kappa,\kappa'}$ denote the radial matrix elements which serve as relative weights of dipole-allowed transitions. Equation (8) shows explicitly the interplay between the angular matrix elements, e.g., the dipole selection rules, and the final-state phase differences.

From bare electronic structure calculations using the local density approximation (LDA) approach, the description of the surface potential is insufficient. Hence, it has been known for a long time that the LDA, and gradient-corrected schemes as well, are not able to provide the correct asymptotic of a potential away from the crystal surface. Therefore, a surface potential derived from density-functional theory (DFT) gives only a good description for surface states which are located near the Fermi energy. This is not, however, a general shortcoming of the DFT. It has been demonstrated, e.g., by Gunnarsson *et al.* [56,57] that in the weighted-density approximation a model function describing the shape of the exchange-correlation hole can be tuned in such a way as to fulfill several physically important limiting conditions, including the $1/z$ asymptotics of the potential outside a solid surface. The *ab initio calculations* incorporating the weighted-density approximation remain, however, relatively rare and have not yet been, to our knowledge, successfully applied to the study of surface-related states. So far, an *ad hoc* adjustment of the potential barrier near the surface remains an arguably workable alternative. A realistic description of the surface potential is given through a spin-dependent Rundgren-Malmström barrier [58] which connects the asymptotic regime $z < z_A$ to the bulk muffin-tin zero V_{or} by a third-order polynomial in z, spanning the range $z_A < z < z_E$. In other words z_E defines the point where the surface region ends and the bulk region starts, at which z_I defines the position of the classical image plane.

In order to substantiate the theoretical discussion we present the theoretical approach in more detail. The surface contribution $I^{\mathrm{surf}}(\epsilon_f,\mathbf{k}_\parallel)$ which is part of the total photocurrent accounts explicitly for surface related spectral features:

$$I^{\mathrm{surf}}(\epsilon_f,\mathbf{k}_\parallel) = -\frac{1}{\pi}\,\mathrm{Im}\int d\mathbf{r}\Psi_f^{*\mathrm{surf}}(\mathbf{r})\triangle\Psi_i^{\mathrm{surf}}(\mathbf{r}), \quad (9)$$

with

$$\Psi_i^{\mathrm{surf}}(\mathbf{r}) = \int d\mathbf{r}' G^+_{1\mathrm{surf}}(\mathbf{r},\mathbf{r}')\triangle^*\Psi_f^{\mathrm{surf}}(\mathbf{r}'). \quad (10)$$

Here, $G^+_{1\mathrm{surf}}$ denotes the retarded Green function of the initial state in the surface region and Δ is the corresponding dipole operator. In the case of a z-dependent barrier potential $V_B = V_B(z)$, the initial- and final-state wave fields have to be calculated numerically in the surface region. Both wave fields $\Psi_i^{\mathrm{surf}}(\mathbf{r})$ and $\Psi_f^{\mathrm{surf}}(\mathbf{r})$ can be decomposed into z-dependent and corresponding parallel components,

$$\Psi_i^{\mathrm{surf}}(\mathbf{r}) = \sum_{\mathbf{g}} \phi_{1\mathbf{g}}(z)e^{i\mathbf{k}_{1\mathbf{g}\parallel}(\mathbf{r}-\mathbf{c}_1)_\parallel}, \quad (11)$$

$$\Psi_f^{\mathrm{surf}}(\mathbf{r}) = \sum_{\mathbf{g}} \psi_{2\mathbf{g}}(z)e^{i\mathbf{k}_{2\mathbf{g}\parallel}(\mathbf{r}-\mathbf{c}_1)_\parallel}, \quad (12)$$

with the regular solutions of the Schrödinger equation $\phi_{1\mathbf{g}}$ and $\psi_{2\mathbf{g}}$ to the reciprocal lattice vector $\mathbf{g}$ for $V_B(z)$ in the range $-\infty < z < c_{1z}$. The value c_{1z} defines the point, where the surface potential goes smoothly into the inner potential of the bulk crystal. This way all matrix-element effects concerning surface-related electronic states are quantitatively considered, Also multiple scattering effects in the surface region are quantitatively described by our approach because all multiple scattering effects between the semi-infinte bulk and the surface potential are considered through the layer-doubling technique [51], which allows one to couple the scattering matrix of the surface potential to the rest bulk. Last, spin-flip processes caused by multiple scattering are quantitatively considered due to the fully relativistic description used in our theory.

C. Computational details

Self-consistent electronic structure calculations were performed within the *ab initio* framework of spin-density functional theory. The Vosko, Wilk, and Nusair parametrization for the exchange and correlation potential was used [59]. The electronic structure was calculated in a fully relativistic mode by solving the corresponding Dirac equation. This was achieved using the relativistic multiple-scattering or KKR formalism in the tight-binding KKR mode [60–62]. The resulting half-space electronic structure represented by single-site scattering matrices for the different layers and the corresponding wave functions for initial- and final-state energies were used as input quantities for the corresponding photocurrent calculations. Lifetime effects in the initial states have been included via a small constant imaginary value of $V_i(E_i) = 0.08$ eV to represent scattering events by structural disorder and other incoherent processes, such as impurity scattering. The higher background appearing in the calculated spectra is due to the presence of the bulk states, which start to disperse at about 0.2 eV binding energy. As a consequence the

theoretical line width of the TSS seems to be broader than the experimental ones.

III. RESULTS AND DISCUSSION

Figure 1(a) sketches the experimental geometry where light incidence and photoelectron detection are in the xz plane. The mirror planes of the crystal lattice are oriented along the $\overline{\Gamma M}$ directions (yz plane). This means that for the presented experiments it is oriented perpendicular to the optical plane of the measurement geometry while the $\overline{\Gamma K}$ direction lies in the optical plane. As a result the photoelectron spin polarization $\mathbf{P} = (P_x, P_y, P_z)$ is only mildly restricted by symmetry and, generally, all components may be nonzero [39]. Figure 1(b) shows ARPES data of the topological surface state obtained at a photon energy of $h\nu = 22$ eV along the $\overline{\Gamma K}$ direction. The upper part of the Dirac cone is visible with the Dirac point at a binding energy of roughly 200 meV.

Due to the spin-orbit coupled nature of the wave function of the topological surface state, expressed by $\psi_k = a\phi_{\uparrow k}(\mathbf{r})|\uparrow\rangle + b\phi_{\downarrow k}(\mathbf{r})|\downarrow\rangle$, the spin polarization may, in general, vary with position $\mathbf{r}$ and wave vector k. This is confirmed by *ab initio* calculations for Bi_2Te_3 [15,63]. The spatially averaged spin polarization is expected to be oriented tangentially to the Fermi surface, i.e., in-plane and perpendicular to the wave vector, along $\overline{\Gamma M}$ while it may develop and additional out-of-plane component along $\overline{\Gamma K}$ [64].

Spin-resolved energy distribution curves (EDCs) $I_{\uparrow\downarrow}(E)$ for the topological surface state are shown in Figs. 1(c) and 1(d) obtained with photon energies of $h\nu = 22$ eV and $h\nu = 27$ eV, respectively. Measured and calculated EDCs at positive and negative wave vectors along k_x for all three spin components P_x, P_y, and P_z are directly compared. The corresponding experimental and theoretical spin polarizations $P(E)$ are displayed in Fig. 2. The hatched areas in Fig. 1(b) indicate the position of the EDC along k_x and the k resolution of the measurements. Focusing first on the experimental results we observe sizable spin polarizations along the y axis that switch sign at opposite wave vectors. These tangential spin components, oriented perpendicular to the wave vector, are in line with the expected intrinsic spin polarization of the topological surface state. However, we also observe spin polarizations along the x axis that are of similar magnitude. Such radial spin components, oriented parallel to the wave vector, should vanish in the spin polarization of the ground state along high-symmetry directions. They can, however, arise from the photoemission process and have also been found for $Bi_2Se_3(0001)$ [22,26]. The measured radial components have the same sign at $+k_x$ and at $-k_x$ for $h\nu = 22$ eV. Furthermore, they show a pronounced photon energy dependence becoming considerably reduced at $h\nu = 27$ eV. On the other hand, the measured spin polarization along z vanishes at both photon energies within experimental uncertainty. For the intrinsic spin polarization a finite out-of-plane component P_z is expected along $\overline{\Gamma K}$. At binding energies of about $E - E_F < -200$ meV

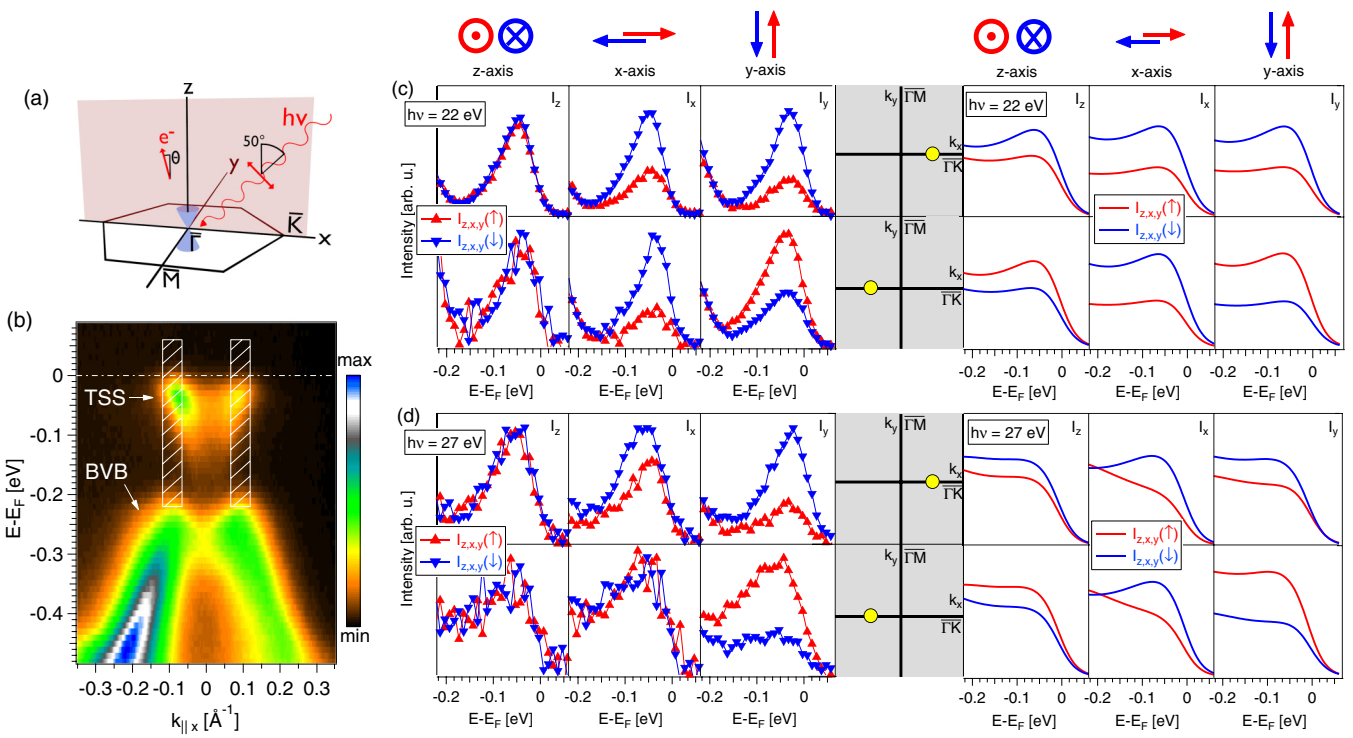

FIG. 1. (a) Sketch of the experimental geometry. The optical plane (xz plane) is colored. (b) ARPES data for $Bi_2Te_3(0001)$ along the $\overline{\Gamma K}$ direction (k_x) showing the topological surface state (TSS) and the topmost bulk valence band (BVB) (p-polarized light, $h\nu = 22$ eV, $T = 50$ K). The hatched rectangles represent the energy range in which the spin-resolved measurements in (c) and (d) were taken and the corresponding k resolution. The dashed line marks the Fermi level E_F. Panels (c) and (d) display measured (left) and calculated (right) spin-resolved energy distribution curves at $h\nu = 22$ eV and $h\nu = 27$ eV (d), respectively. Data for spin-polarization along the x, y, and z axes are presented at positive and negative wave vectors, respectively.

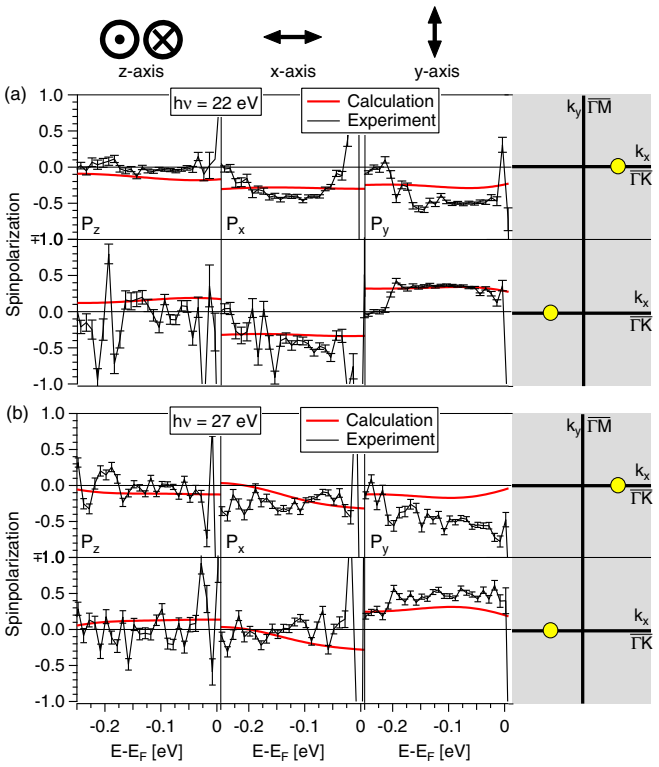

FIG. 2. Calculated (red) and measured (black) photoelectron spin polarization for $Bi_2Te_3(0001)$ at $h\nu = 22$ eV (a) and 27 eV (b), respectively. The data directly corresponds to the according spin-resolved EDC shown in Figs. 1(c)–1(d).

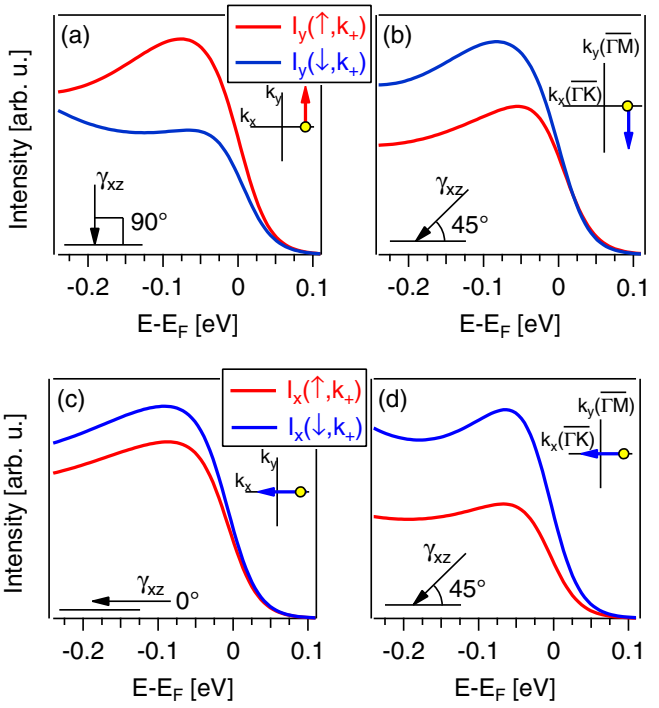

FIG. 3. Calculated spin-resolved EDC at $+k_x$ with the spin-quantization axis along y for vertical (a) and oblique (b) light incidence in the xz plane (p-polarized light, $h\nu = 22$ eV). (c) and (d) show calculated spin-resolved EDC at $+k_x$ with the spin-quantization axis along x for parallel (d) and oblique, 45°, (b) light incidence, respectively. In both cases a dependence of the calculated photoelectron spin polarization on the angle of incidence is apparent.

for all EDCs the onset of the valence band is visible, showing no spin polarization [see Fig. 1(b)].

Comparing our measurements to the calculated spin-resolved EDC, we find an overall good agreement. In particular, our photoemission calculations confirm the appearance of sizable radial spin components of comparable magnitude as for the tangential components. In line with the experiment, the tangential component changes sign for $k_x \rightarrow -k_x$ while the sign of the radial component remains unchanged. Furthermore, our calculations also indicate a reduction of the radial spin component at $h\nu = 27$ eV, albeit not as pronounced as in the experiment. While the out-of-plane spin polarization component P_z is smaller than P_x and P_y, as in the measurements, it is clearly finite. Thus, there appears to be a mild overestimation of P_z in the theoretical results while the tangential components P_y tend to be slightly underestimated. However, the main experimental observation, namely the appearance of photon-energy-dependent radial spin components in the photoelectron spin polarization of the topological surface state, is reproduced by our calculations. We also note an apparent difference in the experimental and theoretical lineshapes of the TSS. In the theoretical spectra lifetime effects in the initial states have been included via a small constant imaginary value of $V_i(E_i) = 0.08$ eV to represent scattering events by structural disorder and other incoherent processes, such impurity scattering. The higher background appearing in the calculated spectra is due to the presence of bulk states, which start to disperse at about 0.2 eV binding energy. As a consequence the theoretical linewidth of the TSS seems to be broader than the experimental ones.

Based on this general agreement between experiment and theory we will now further analyze the effects of the photoemission process on the photoelectron spin polarization. Varying the light incidence angle in our calculations and thereby the light polarization vector $\mathbf{A}$ allows us to address specific orbital components of the initial-state wave functions ψ_i via the dipole matrix element $\langle \psi_f | \mathbf{A} \cdot \mathbf{p} | \psi_i \rangle$, with electron momentum $\mathbf{p}$ and final state ψ_f. In Figs. 3(a) and 3(b) we compare calculated spin-resolved spectra for normal and oblique incidence of p-polarized light in the xz plane, respectively. In the latter case the photoemission signal originates mainly from excitation of p_z orbitals, while in the former case it is dominated by excitation of $p_{x,y}$ orbitals. Evidently, the photoelectron spin polarization along y changes sign between the two experimental geometries as a direct consequence of spin-orbit coupling in the initial-state wave function, namely a preferred excitation of either the $\phi_\uparrow$ part or the $\phi_\downarrow$ part of $\psi_i = a\phi_\uparrow(\mathbf{r})|\uparrow\rangle + b\phi_\downarrow(\mathbf{r})|\downarrow\rangle$. This is in agreement with previous experimental observations and model calculations in Bi_2Se_3 [23,25,26].

In Figs. 3(c) and 3(d) we address the influence of the initial state on the radial components in the photoelectron spin polarization that we observed experimentally. To this end we consider calculated spin-resolved spectra for parallel and oblique incidence of p-polarized light in the xz plane. In the

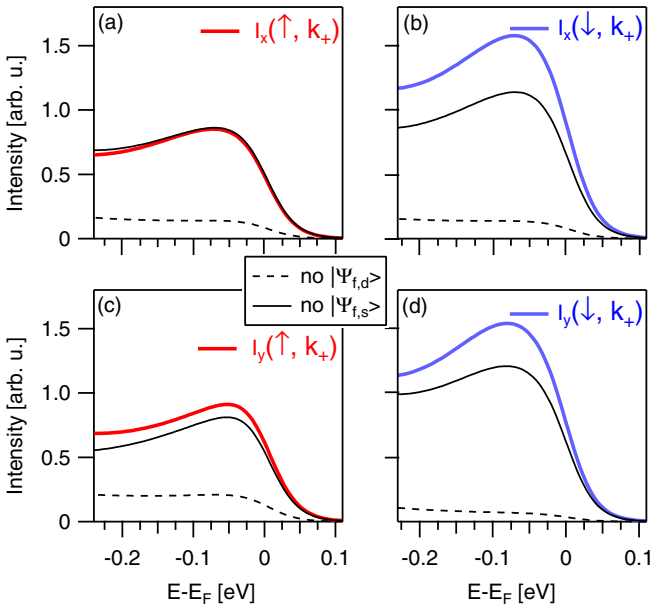

FIG. 4. Calculated spin-resolved EDC at $+k_x$ with the spin-quantization axis along x in (a) and (b) and along y in (c) and (d) ($h\nu = 22$ eV). Red (spin $\uparrow$) and blue (spin $\downarrow$) lines display EDCs for the full final-state wave function [cf. Fig. 1(c)]. The continuous and dashed black lines show calculated EDCs excluding final-state orbitals of s and d character, respectively.

former case the photoemission signal arises almost exclusively from p_z orbitals while in the latter case also $p_{x,y}$ orbitals contribute. When probing only the p_z part of the initial state one might expect influences of the photoemission process to become weaker because the initial-state spin polarization is orbital dependent [25,26,42]. Indeed, our calculations in Figs. 3(c) and 3(d) show a considerably reduced spin polarization along x for parallel light incidence. This confirms that spin-orbit coupling in the initial-state wave functions and experimental geometry play an important role in deviations between ground state and photoelectron spin polarization [26]. The finite radial component in Fig. 3(c) reflects that, along $\overline{\Gamma K}$, both $\phi_\uparrow$ and $\phi_\downarrow$ have contributions from p_z orbitals. We performed additional calculations at higher excitation energies of approximately $h\nu = 1000$ eV (not shown) where the final states should be described well by free-electron states. Also in this case radial components in the spin polarization of similar magnitude were obtained, in agreement with previous model calculations [26].

We will now consider effects in the final state of the photoemission process on the photoelectron spin polarization. As the topological surface state is composed of Bi $6p$ and Te $5p$ orbitals, the relevant final states are of s and d character due to the selection rule $\Delta l = \pm 1$. Figure 4 shows calculated spin-resolved spectra for the radial and the tangential spin components in (a)–(b) and (c)–(d), respectively. In each case we compare calculations with the full final-state wave function and those where s and d orbital contributions are "switched off." Interestingly, for both spin components the behavior in the spin-up and the spin-down channel is rather different. In the spin-down channel s and d final states interfere constructively; that is, the intensity for the full final state is higher than the sum of individual s and d contributions. By contrast, in the spin-up channel s and d final states interfere destructively, as the intensity for the full final state is smaller than the sum of s and d contributions. Hence, our calculations reveal spin-dependent relative phases between s $(l-1)$ and d $(l+1)$ final states that will significantly influence the photoelectron spin polarization in dependence of photon energy, as is expected from Eq. (8). Related spin-dependent effects in the continuum final states are a well-known origin of photoelectron spin polarization in the case of photoexcitation from closed core-level shells [35].

Within the one-step model approach the photoemission intensity distribution, in principle, consists of a product of angular matrix elements weighted with corresponding radial matrix elements, summed up over all spin and orbital degrees of freedom. This summation, restricted through the dipole selection rules, is explicitly seen in Eq. (8), that describes a linear combination of matrix elements containing contributions from different excitation channels simultaneously, as for example transitions from different p-like orbitals in the initial state to s- or d-like final states depending on the excitation energy. Due to spin-orbit interaction the spin and orbital nature of the initial and final states are strongly entangled, which within our theoretical approach is described by spin-flip processes in the relativistic multiple scattering. Finally, the weighted sum over the individual matrix elements, together with the summation over different atomic layers which contribute with exponentially decaying amplitudes according to the inelastic mean free path, may generate considerable deviations between the photoelectron spin polarization and the spin expectation-value in the ground state.

IV. CONCLUSIONS

To conclude we have presented a combined experimental and theoretical study of the photoelectron spin polarization in angle-resolved photoemission from the topological insulator $Bi_2Te_3(0001)$. Considerable deviations between the photoelectron spin polarization and the expected intrinsic spin polarization of the topological surface state are observed experimentally and confirmed by relativistic one-step photoemission calculations. Our theoretical analysis indicates that spin-orbit coupling in the initial-state wave functions, dipole selection rules, and spin-dependent relative phases in the final-state wave functions of different orbital angular momentum affect the photoelectron spin polarization considerably. The present findings, thus, illustrate that a quantitative experimental access to the spin-polarization vector of topological surface states is, in general, not straightforward. It requires a detailed analysis of the photoemission matrix element as well as a careful consideration of experimental parameters on the photoelectron spin polarization, such as setup geometry, photon energy, and photon polarization. This is expected to hold particularly in situations where the wave function of the surface state acquires additional complexity, e.g., due to influences of the in-plane potential landscape at the surface [63,64], or due to hybridization with bulk electronic states [63,65,66] or with other surface states [42].

ACKNOWLEDGMENTS

The synchrotron radiation experiments were performed with the approval of HiSOR (Proposal No. 14-A-55). This work was supported by the Deutsche Forschunsgsgemeinschaft (DFG) through SFB 1170 'Tocotronics', FOR1162 (P3), and SPP 1666 (Project Nr. Eb-154/26), by the BMBF (05K13WMA), by the Grant-in-Aid for Scientific Research (A) 20244045, and by the grant of Saint Petersburg State University for scientific investigations (No. 15.61.202.2015). J.M. would like to acknowledge CENTEM PLUS (LO1402). T.V.K. acknowledges the financial support of the research, which was carried out within the state assignment of FASO of Russia (theme "Electron" No. 01201463326), supported in part by RFBR (Project No. 14-32-50936).

[1] L. Fu, C. L. Kane, and E. J. Mele, Phys. Rev. Lett. **98**, 106803 (2007).
[2] M. Z. Hasan and C. L. Kane, Rev. Mod. Phys. **82**, 3045 (2010).
[3] X.-L. Qi and S.-C. Zhang, Rev. Mod. Phys. **83**, 1057 (2011).
[4] F. Ortmann, S. Roche, and S. O. Valenzuela, *Topological Insulators: Fundamentals and Perspectives* (John Wiley & Sons, New York, 2015).
[5] Y. Xia, D. Qian, D. Hsieh, L. Wray, A. Pal, H. Lin, A. Bansil, D. Grauer, Y. S. Hor, R. J. Cava *et al.*, Nat. Phys. **5**, 398 (2009).
[6] Y. L. Chen, J. G. Analytis, J.-H. Chu, Z. K. Liu, S.-K. Mo, X. L. Qi, H. J. Zhang, D. H. Lu, X. Dai, Z. Fang *et al.*, Science **325**, 178 (2009).
[7] D. Hsieh, Y. Xia, L. Wray, D. Qian, A. Pal, J. H. Dil, J. Osterwalder, F. Meier, G. Bihlmayer, C. L. Kane *et al.*, Science **323**, 919 (2009).
[8] J. H. Dil, J. Phys.: Condens. Matter **21**, 403001 (2009).
[9] D. Hsieh, Y. Xia, D. Qian, L. Wray, J. H. Dil, F. Meier, J. Osterwalder, L. Patthey, J. G. Checkelsky, N. P. Ong *et al.*, Nature (London) **460**, 1101 (2009).
[10] A. Nishide, A. A. Taskin, Y. Takeichi, T. Okuda, A. Kakizaki, T. Hirahara, K. Nakatsuji, F. Komori, Y. Ando, and I. Matsuda, Phys. Rev. B **81**, 041309 (2010).
[11] S. Souma, K. Kosaka, T. Sato, M. Komatsu, A. Takayama, T. Takahashi, M. Kriener, K. Segawa, and Y. Ando, Phys. Rev. Lett. **106**, 216803 (2011).
[12] Z.-H. Pan, E. Vescovo, A. V. Fedorov, D. Gardner, Y. S. Lee, S. Chu, G. D. Gu, and T. Valla, Phys. Rev. Lett. **106**, 257004 (2011).
[13] K. Miyamoto, A. Kimura, T. Okuda, H. Miyahara, K. Kuroda, H. Namatame, M. Taniguchi, S. V. Eremeev, T. V. Menshchikova, E. V. Chulkov *et al.*, Phys. Rev. Lett. **109**, 166802 (2012).
[14] H. Mirhosseini and J. Henk, Phys. Rev. Lett. **109**, 036803 (2012).
[15] A. Herdt, L. Plucinski, G. Bihlmayer, G. Mussler, S. Döring, J. Krumrain, D. Grützmacher, S. Blügel, and C. M. Schneider, Phys. Rev. B **87**, 035127 (2013).
[16] M. Nomura, S. Souma, A. Takayama, T. Sato, T. Takahashi, K. Eto, K. Segawa, and Y. Ando, Phys. Rev. B **89**, 045134 (2014).
[17] Y. H. Wang, D. Hsieh, D. Pilon, L. Fu, D. R. Gardner, Y. S. Lee, and N. Gedik, Phys. Rev. Lett. **107**, 207602 (2011).
[18] G. Bian, L. Zhang, Y. Liu, T. Miller, and T.-C. Chiang, Phys. Rev. Lett. **108**, 186403 (2012).
[19] M. R. Scholz, J. Snchez-Barriga, J. Braun, D. Marchenko, A. Varykhalov, M. Lindroos, Y. J. Wang, H. Lin, A. Bansil, J. Minr *et al.*, Phys. Rev. Lett. **110**, 216801 (2013).
[20] M. Ärrälä, J. Nieminen, J. Braun, H. Ebert, and M. Lindroos, Phys. Rev. B **88**, 195413 (2013).
[21] A. Crepaldi, F. Cilento, M. Zacchigna, M. Zonno, J. C. Johannsen, C. Tournier-Colletta, L. Moreschini, I. Vobornik, F. Bondino, E. Magnano *et al.*, Phys. Rev. B **89**, 125408 (2014).
[22] C. Jozwiak, Y. L. Chen, A. V. Fedorov, J. G. Analytis, C. R. Rotundu, A. K. Schmid, J. D. Denlinger, Y.-D. Chuang, D.-H. Lee, I. R. Fisher *et al.*, Phys. Rev. B **84**, 165113 (2011).
[23] C. Jozwiak, C.-H. Park, K. Gotlieb, C. Hwang, D.-H. Lee, S. G. Louie, J. D. Denlinger, C. R. Rotundu, R. J. Birgeneau, Z. Hussain *et al.*, Nat. Phys. **9**, 293 (2013).
[24] J. Sánchez-Barriga, A. Varykhalov, J. Braun, S.-Y. Xu, N. Alidoust, O. Kornilov, J. Minár, K. Hummer, G. Springholz, G. Bauer *et al.*, Phys. Rev. X **4**, 011046 (2014).
[25] Z. Xie, S. He, C. Chen, Y. Feng, H. Yi, A. Liang, L. Zhao, D. Mou, J. He, Y. Peng *et al.*, Nat. Commun. **5**, 3382 (2014).
[26] Z.-H. Zhu, C. Veenstra, S. Zhdanovich, M. Schneider, T. Okuda, K. Miyamoto, S.-Y. Zhu, H. Namatame, M. Taniguchi, M. Haverkort *et al.*, Phys. Rev. Lett. **112**, 076802 (2014).
[27] E. E. Krasovskii, J. Phys.: Condens. Matter **27**, 493001 (2015).
[28] U. Fano, Phys. Rev. **178**, 131 (1969).
[29] U. Heinzmann, J. Kessler, and J. Lorenz, Phys. Rev. Lett. **25**, 1325 (1970).
[30] D. T. Pierce and F. Meier, Phys. Rev. B **13**, 5484 (1976).
[31] N. A. Cherepkov, J. Phys. B: At. Mol. Phys. **12**, 1279 (1979).
[32] U. Heinzmann, J. Phys. B **13**, 4353 (1980).
[33] J. Kessler, *Polarized Electrons*, Springer Series on Atoms and Plasmas, Vol. 1 (Springer, Berlin, 1985).
[34] H. B. Rose, A. Fanelsa, T. Kinoshita, C. Roth, F. U. Hillebrecht, and E. Kisker, Phys. Rev. B **53**, 1630 (1996).
[35] U. Heinzmann and J. H. Dil, J. Phys.: Condens. Matter **24**, 173001 (2012).
[36] J. Kirschner, R. Feder, and J. F. Wendelken, Phys. Rev. Lett. **47**, 614 (1981).
[37] A. Kimura, E. E. Krasovskii, R. Nishimura, K. Miyamoto, T. Kadono, K. Kanomaru, E. V. Chulkov, G. Bihlmayer, K. Shimada, H. Namatame *et al.*, Phys. Rev. Lett. **105**, 076804 (2010).
[38] J. M. Riley, F. Mazzola, M. Dendzik, M. Michiardi, T. Takayama, L. Bawden, C. Granerd, M. Leandersson, T. Balasubramanian, M. Hoesch *et al.*, Nat. Phys. **10**, 835 (2014).
[39] J. Henk, A. Ernst, and P. Bruno, Phys. Rev. B **68**, 165416 (2003).
[40] H. Mirhosseini, J. Henk, A. Ernst, S. Ostanin, C.-T. Chiang, P. Yu, A. Winkelmann, and J. Kirschner, Phys. Rev. B **79**, 245428 (2009).
[41] O. V. Yazyev, J. E. Moore, and S. G. Louie, Phys. Rev. Lett. **105**, 266806 (2010).
[42] H. Bentmann, S. Abdelouahed, M. Mulazzi, J. Henk, and F. Reinert, Phys. Rev. Lett. **108**, 196801 (2012).

[43] S. N. P. Wissing, A. B. Schmidt, H. Mirhosseini, J. Henk, C. R. Ast, and M. Donath, Phys. Rev. Lett. **113**, 116402 (2014).
[44] H. Maaß, H. Bentmann, C. Seibel, C. Tusche, S. V. Eremeev, T. R. F. Peixoto, O. E. Tereshchenko, K. A. Kokh, E. V. Chulkov, J. Kirschner, and F. Reinert, Nat. Commun. **7**, 11621 (2016).
[45] T. Okuda, K. Miyamaoto, H. Miyahara, K. Kuroda, A. Kimura, H. Namatame, and M. Taniguchi, Rev. Sci. Instrum. **82**, 103302 (2011).
[46] K. A. Kokh, S. V. Makarenko, V. Golyashov, O. A. Shegai, O. E. Tereshchenko, CrystEngComm **16**, 581 (2014).
[47] T. Okuda, K. Miyamoto, A. Kimura, H. Namatame, and M. Taniguchi, J. Electron Spectrosc. Relat. Phenom. **201**, 23 (2015).
[48] J. B. PendrySurf. Sci. **57**, 679 (1976).
[49] G. Borstel, Appl. Phys. A **38**, 193 (1985).
[50] C. Caroli, D. Lederer-Rozenblatt, B. Roulet, and D. Saint-James, Phys. Rev. B **8**, 4552 (1973).
[51] J. B. Pendry, *Low Energy Electron Diffraction* (Academic, London, 1974).
[52] J. Braun, Rep. Prog. Phys. **59**, 1267 (1996).
[53] J. Braun, in *Band-Ferromagnetism: Ground-State and Finite-Temperature Phenomena*, edited by K. Baberschke, M. Donath and W. Nolting (Springer, Berlin, 2001), p. 267.
[54] G. Hilgers, M. Potthoff, N. Müller, U. Heinzmann, L. Haunert, J. Braun, and G. Borstel, Phys. Rev. B **52**, 14859 (1995).
[55] G. Schönhense, Phys. Scr. **31**, 255 (1990).
[56] O. Gunnarsson, M. Jonson, and B. I. Lundqvist, Phys. Rev. B **20**, 3136 (1979).
[57] R. O. Jones and O. Gunnarsson, Rev. Mod. Phys. **61**, 689 (1989).
[58] G. Malmström and J. Rundgren, Comput. Phys. Commun. **19**, 263 (1980).
[59] S. H. Vosko, L. Wilk, and M. Nusair, Can. J. Phys. **58**, 1200 (1980)
[60] H. Ebert, in *Electronic Structure and Physical Properties of Solids*, edited by H. Dreyssé, Lecture Notes in Physics Vol. 535 (Springer, Berlin, 2000), p. 191.
[61] H. Ebert, D. Ködderitzsch, and J. Minár, Rep. Prog. Phys. **74**, 096501 (2012)
[62] H. Ebert *et al.*, The Munich SPR-KKR package, version 6.3, http://olymp.cup.uni-muenchen.de/ak/ebert/SPRKKR (2012).
[63] J. Henk, A. Ernst, S. V. Eremeev, E. V. Chulkov, I. V. Maznichenko, and I. Mertig, Phys. Rev. Lett. **108**, 206801 (2012).
[64] L. Fu, Phys. Rev. Lett. **103**, 266801 (2009).
[65] H. Bentmann and F. Reinert, New J. Phys. **15**, 115011 (2013).
[66] C. Seibel, H. Bentmann, J. Braun, J. Minár, H. Maaß, K. Sakamoto, M. Arita, K. Shimada, H. Ebert, and F. Reinert, Phys. Rev. Lett. **114**, 066802 (2015).